With increasing pressure the first-order AFE-PE transitions in $PbZrO_3$ and $PbHfO_3$ acquire the characteristics of second-order transitions. These effects undoubtedly reflect important pressure-induced changes in the ionic displacements accompanying these transitions.

ACKNOWLEDGMENTS

Low-Temperature Behavior of a Pure Dipole-Dipole System

PAUL H. E. MEIJER

Catholic University of America, Washington, D. C. 20017

and

National Bureau of Standards, Washington, D. C. 20234

AND

DAVID J. O'KEEFFE

Naval Ordnance Laboratory, White Oak, Maryland

(Received 1 December 1969)

The Van Vleck moment expansion is applied to a pure dipole system. On the basis of the long-range nature of the forces, sequences of diagrams are selected that give the dominant contributions in the lattice sums. A selection of diagrams contributing to the entropy and susceptibility is displayed. There are three different summations to be performed for each type of diagram: the trace over the spin variables, the lattice summation, and the summation over the Cartesian coordinates. The second was performed on a computer, and the last is obtained by means of the Kramers-Wannier diagonalization. In order, to obtain the contributions of diagrams of higher order, a Fourier transform is employed. The calculations are performed for cerous magnesium nitrate using a g factor that is zero along the c axis. The results are compared with experiments. The susceptibility χ was calculated for a uniform and for a nonuniform field, and it is suggested that the critical temperature is determined by the infinity of $\chi(q)$ for $q \neq 0$, rather than by that of $\chi(0)$.

I. GENERAL CONSIDERATIONS

IN order to predict a critical point T_c and the state of magnetization below T_c, one needs a complete set of parameters to describe the magnetic system. They are:

(a) The lattice structure—the type of crystal structure and the actual lengths and orientations of the lattice vectors **a**, **b**, **c**, as well as the parameters u, v, etc., describing the atoms in the unit cell, if more than one.

(b) The g factors, more specifically the tensors, one for each atom per unit cell.

(c) The interaction as a function of the relative distance $J(r_{ij})$, which in general can be of the tensorial type, i.e., not necessarily dependent on the distance only.

Suppose all these data were available, how can we go about determining the critical temperature?

Before answering this question let us take a look at the availability of the data just mentioned. As far as (a) is concerned a sufficient amount of good data is usually available from x-ray work. The only practical trouble is that the lattice parameters are not always determined at the temperature range one is interested in and although the changes at low temperatures are usually minute, the coefficients to be calculated later are very sensitive to the values of the parameters.

The g factors are also sufficiently known in most cases. The values of $g_\perp$ and $g_{\parallel}$ as well as the axis with respect to which they are parallel and perpendicular are very often known from paramagnetic resonance experiments in diluted crystals.

The third quest for data, the interaction as a function of the relative distance is the weakest link in the chain. Although recently a number of successful experiments have been performed to determine the nearest- and next-nearest-neighbor interactions between paramagnetic ions from satellite lines in a number of moderately diluted crystals,[1] the data are far from complete. There is one exception, however, the salts in which the dipole-dipole interaction is dominant. It is reasonable to assume that the permeability of an insulator is the same as that of the vacuum and although occasionally pseudo-dipole forces have been proposed[2] one feels that the use of the "free" dipole-dipole interaction is a good description in cases where the exchange forces seem to be weak. It is much less clear that higher multipole forces should not be taken into account.

The attraction to study the case of dominant dipolar forces as a challenge for the theory is clear: Here one

---

[1] See, for instance, M. T. Hutchings, R. J. Birgeneau, and W. P. Wolf, Phys. Rev. **168**, 1026 (1968); **179**, 275 (1969).

[2] J. H. Van Vleck and J. van Kranendonck, Rev. Mod. Phys. **30**, 1, (1958).

can pretend that the interaction is known and it is up to the theory to predict the critical point.

From the point of view of the theory, however, the situation is much less appealing. Almost all theories are approximations; the only exception is of no use, since it deals with an Ising interaction between nearest neighbors in a two-dimensional model. To what extent approximate theories are useful depends of course on the number of steps, terms, or iterations necessary to obtain a reasonable result. However, most theories need an assumption about the magnetic state the system condenses into: ferromagnetic, antiferromagnetic, or, in general, some kind of staggered magnetic structure. Moreover, if a guess can be made for the ground state, it is not yet sure whether this state will be identical with the state just below the highest critical point. The uncertainty about the magnetic state stems from the fact that the dipole interaction has both signs, depending on the direction.

The methods presently at our disposition are:

(a) The molecular field method.

(b) The cluster variation method. A minimization of the free energy of a cluster in which the environment is treated as an effective field. The simplest form is the Oguchi constant coupling method.

(c) Low-temperature expansions either by flipping one spin at a time as in the Ising model or by spin waves.

(d) Green's functions, a combination of spin waves and molecular field methods.

(e) High-temperature expansion or the Van Vleck moment method.

For all these methods except the last, one has to know the ground state, since this state is completely unknown for a pure dipole-dipole system. Hence the calculation was performed with the Van Vleck method.

II. DISCUSSION OF PREVIOUS WORK

What has been done before? Lorentz pointed out[3] that the dipole-dipole forces cancel out in cubic symmetry and in a spherical sample. This leads to the result that the leading term in the specific heat is equal to zero, which we used as a test case. Lorentz's calculation was actually done for induced dipoles, but the result holds for permanent dipoles as well.

Second, Luttinger and Tisza[4] determined the ground state by a combination of cluster method and an almost correct diagonalization. The technique used is formulated as replacing a strong constraint by a weak constraint, and is identical to the sphericalization method applied to a cluster rather than to the whole system. The major drawback of their conclusion (an antiferromagnetic ground state) is that the magnetic periodicity is *a priori* fixed. Hence one cannot expect much else

than either a ferromagnetic or an antiferromagnetic ground state. If the ground state is ferromagnetic, then the magnetization will depend on the shape. It is, moreover, possible that the ground state is not homogeneous, that it would consist of domains; it is extremely difficult to prove that this is not so.

In 1952 Lax[5] described the behavior of a dipole-dipole system in the spherical approximation. He found an ordered state at low temperature. He did not compute the k value of this state, since he remained critical of the spherical-model assumption.

The first few terms in the high-temperature expansion were calculated by Daniels et al. in 1953.[6] The $(1/kT)^2$ term in the specific heat and the Curie-Weiss Δ in the susceptibility were explicitly calculated for cerium magnesium nitrate (CMN) and a number of other salts with pure or predominant dipole-dipole interaction. This paper also contains the algebra for the next higher-order terms.

In 1964 Daniels and Felsteiner did a Luttinger-Tisza calculation for CMN. Lattice sums were again calculated by Peverley and Meijer to obtain the dependence on small changes in the lattice constants.

Recently Wong, Dembinski, and Opechowski[7] obtained the dependence on $g_\perp/g_{||}$ which is expressed in a power series in this quantity.

The recent experimental work[8-12] has been reviewed by Hudson.[13]

III. VAN VLECK MOMENT EXPANSION

The first extensive calculation of the partition function of a paramagnetic salt was done by Van Vleck in 1937. The method can be further improved by using the results of the diagrammatic method.

The partition function in a high-temperature expansion is given by ($\beta = 1/KT$):

$$Z = \mathrm{Tr} \sum_{n=0}^{\infty} \frac{(-\beta \mathcal{3C})^n}{n!}, \qquad (3.1)$$

where the trace has to be taken with respect to all the spins in the Hamiltonian. The detailed form of the Hamiltonian will be described below. It is convenient

[3] H. A. Lorentz, *The Theory of Electrons* (Teubner, Leipzig, 1909), Sec. 117.

[4] J. M. Luttinger and L. Tisza, Phys. Rev. **70**, 954 (1946).

[5] M. Lax, J. Chem. Phys. **20**, 1351 (1952). See also R. Rosenberg and M. Lax [*ibid.* **21**, 424 (1953)] who calculated the susceptibility up to T^{-4} for cubic lattices.

[6] J. M. Daniels, Proc. Phys. Soc. (London) **A64**, 673 ,(1953); and J. M. Daniels and J. Felsteiner, Can. J. Phys. **A42**, 1469 (1964).

[7] S. Wong, S. T. Dembinski, and W. Opechowski, Physica **42**, 565 (1969).

[8] R. P. Hudson and R. S. Kaeser, Physics **3**, 95 (1967).

[9] K. W. Mess, J. Lubbers, L. Niesen, and W. J. Huiskamp, Physica **41**, 260 (1969)

[10] W. R. Abel, A. C. Anderson, W. C. Black, and J. C. Wheatley, Phys. Rev. **147**, 111 (1966).

[11] B. M. Abraham and Y. Eckstein, Phys. Rev. Letters **20**, 649 (1968).

[12] D. J. Abeshouse, G. O. Zimmerman, D. R. Kelland, and E. Maxwell, Phys. Rev. Letters **23**, 308 (1969).

[13] R. P. Hudson, Cryogenics **9**, 76 (1969).

to introduce the symbol $\langle \ \rangle$:

$$\langle \rho \rangle = \mathrm{Tr}\rho/(\mathrm{Tr}1),$$

where ρ is an arbitrary function of the spin operators and 1 the unit matrix in $(2S+1)^N$-dimensional spin space. N is the total number of spins. In this notation we find

$$\ln Z = N \ln\left(1 + \sum_{n=1}^{\infty} \frac{\langle -\beta\mathcal{H}\rangle^n}{n!}\right). \quad (3.2)$$

The second term can be expressed in a semi-invariant expansion

$$\ln Z = N \ln(2S+1) + \sum_{n=1}^{\infty} \frac{(-\beta)^n}{n!} M_n, \quad (3.3)$$

where the semi-invariants or cumulants are given by

$$M_n = n! \sum_{\{n_i\}} (-1)^{\Sigma n_i - 1}(\Sigma n_i - 1)!\Pi\left[\frac{1}{n_i}\left(\frac{\langle \mathcal{H}^i \rangle}{i!}\right)^{n_i}\right]$$

or simply by the statement that one should omit all disconnected diagrams. The leading diagram has weight factor 1:

$$M_n = \langle \mathcal{H}^n \rangle_{\mathrm{conn}}.$$

From this, one can obtain the entropy

$$S/Nk - \ln(2S+1) \equiv \sigma = -\frac{1}{N}\sum \frac{n-1}{n!}(-\beta)^n M_n \quad (3.4)$$

and the susceptibility tensor $\chi^{\alpha\beta}$

$$\beta\chi^{\alpha\beta} = \lim_{H \to 0} \frac{1}{H^\alpha}\left(\frac{\partial \ln Z}{\partial H^\beta}\right)_T \quad (3.5)$$

in a straightforward way. $\mathbf{H}$ is the magnetic field, with components H^α.

The Hamiltonian consists of three parts:

$$\mathcal{H}_e = \sum_{i<j} J_{ij}^{(e)} S_i S_j, \quad (3.6a)$$

$$\mathcal{H}_D \equiv \sum_{i<j} \left[(\mu_i\mu_j)/r_{ij}^3 - 3(\mu_i r_{ij})(\mu_j r_{ij})/r_{ij}^5\right], \quad (3.6b)$$

$$\mathcal{H}_z = -\mathbf{H}\cdot\mathbf{\mu}, \quad (3.6c)$$

where $\mathcal{H}_e$ is the exchange interaction between nearest, next nearest, etc., neighbors. The dipole interaction $\mathcal{H}_D$ and the Zeeman interaction $\mathcal{H}_z$ are expressed in the magnetic moment $\mathbf{\mu}$ of the ion. This moment depends on the spin (or in the case of many rare-earth ions rather on the effective spin) via the g tensor:

$$\mu_i^\alpha = \mu_B g_i^{\alpha\beta} S_i^\beta \quad (\alpha,\beta = x,y,z). \quad (3.7)$$

This leads to the following expression for $\mathcal{H}_D$:

$$\mathcal{H}_D = \sum_{i<j} 4P_{ij}^{\alpha\beta} S_i^\alpha S_j^\beta, \quad (3.8)$$

where

$$P_{ij}^{\alpha\beta} = \tfrac{1}{4}\mu_B^2\left(\frac{g_i^{\sigma\alpha} g_j^{\sigma\beta}}{r_{ij}^3} - \frac{3g_i^{\alpha\lambda} g_j^{\beta\lambda} r_{ij}^\lambda r_{ij}^\lambda}{r_{ij}^5}\right) \quad (3.9)$$

as was pointed out by Daniels.[6] In almost all cases (the notable exceptions are the Tutton salts) the g tensor is independent of the position i.

In the case of cerous magnesium nitrate one can (a) neglect the exchange interaction, (b) use an effective spin $S = \tfrac{1}{2}$, and (c) take $g_{||}$ equal to zero.

A short discussion on the shape dependence is in order. The internal magnetization will be homogeneous only if the sample has an ellipsoidal shape. If the sample has an arbitrary shape it generally is assumed that it will break up in homogeneously magnetized domains although no firm proof exists. Shape dependence from one ellipsoidal form to another can be calculated by means of demagnetization factors. The zero-field behavior is shape-independent, that is, the critical point and the magnetization above T_c presumably contain only terms that converge unconditionally. Below T_c the magnetization curve may depend on the shape. Whether it does so can be investigated by looking at the conditionally convergent terms in the high-temperature expansion.[14]

IV. DIAGRAMS OF HIGH-TEMPERATURE EXPANSION

The expression

$$\mathcal{H}^n = (\mathcal{H}_D + \mathcal{H}_z)^n \quad (4.1)$$

contains two types of terms: One term: $\mathcal{H}_D{}^n$ is the sole contribution to the zero-field specific heat. A set of terms containing $n-2$ factors $\mathcal{H}_D$ and two factors $\mathcal{H}_z$ will determine the susceptibility. In order to calculate the latter, one has to realize that the two parts of the Hamiltonian do not commute with each other. There are $\tfrac{1}{2}n(n-1)$ positions of the two $\mathcal{H}_z$'s between the $\mathcal{H}_D$'s. Using the cyclic property of the trace there are:

(i) If n is even: $\tfrac{1}{2}n$ different traces, each occurring n times except the one where $\mathcal{H}_z$ is sandwiched between an equal number of $\mathcal{H}_D$'s (on a circle); this term occurs only $\tfrac{1}{2}n$ times.

(ii) If n is odd: $\tfrac{1}{2}(n-1)$ different traces, each occurring n times.

If one needed to calculate the off-diagonal elements of $\chi^{\alpha\beta}$ one would need to take into account the fact that the two Zeeman terms do not commute. Here, however, we need the diagonal parts only, since $g_{||} \approx 0$ we have $\chi^{zz} = \chi^{xz} = \chi^{yz} = 0$ and $\chi^{xy} \approx 0$ on the basis of symmetry (one can show that only one layer contributes to χ_{xy}).

The Hamiltonian parts $\mathcal{H}_D$ and $\mathcal{H}_z$ commute with themselves, but one has to be very careful about a product of factors of a given configuration (i.e., a

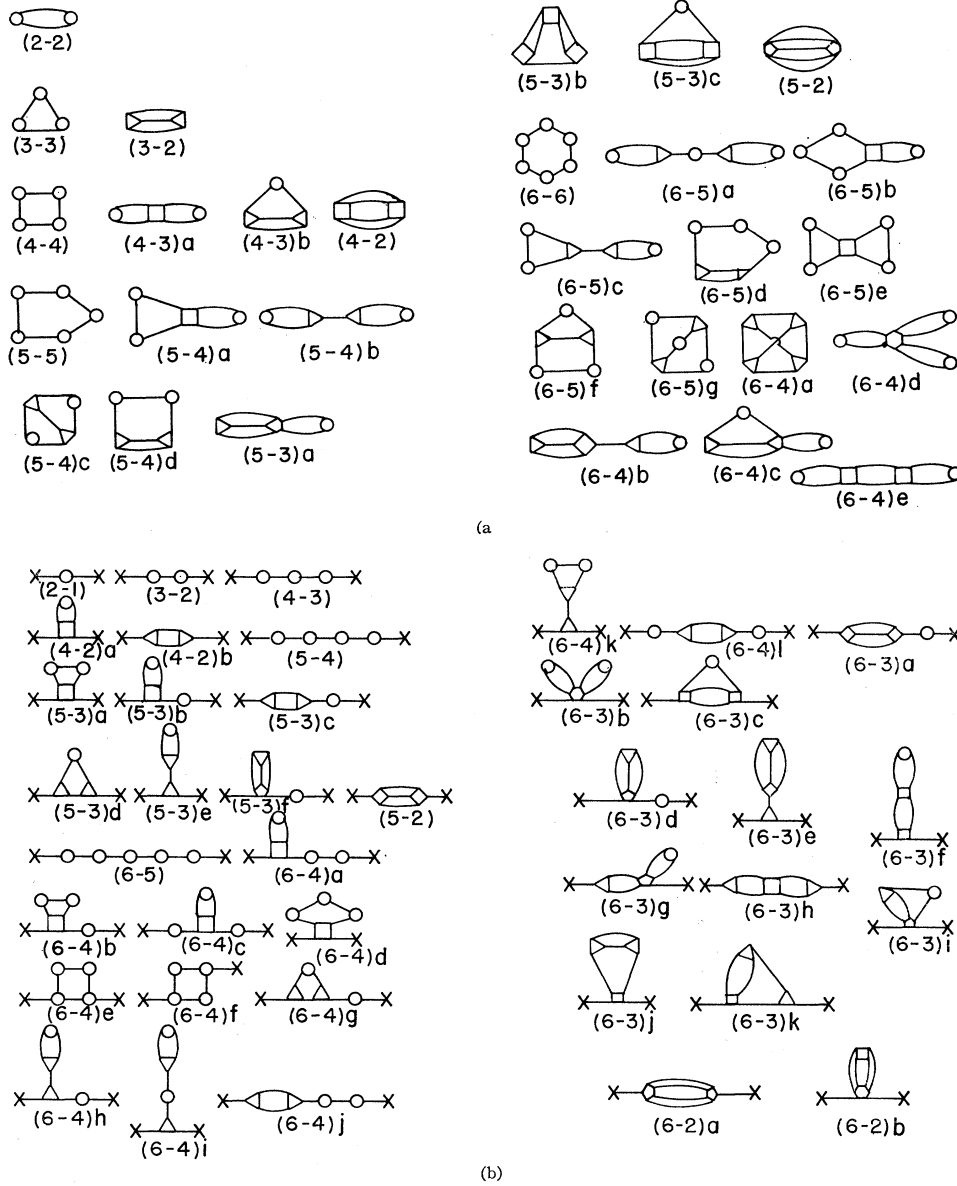[14] P. M. Levy, Phys. Rev. **170**, 595 (1968).

(a

(b)

FIG. 1 (a). Diagrams contributing to the entropy. (b) Diagrams contributing to the susceptibility.

diagram). Here the order of the factors is as important as the individual terms of the series contained in $\mathcal{K}_D{}^n$ do not commute. To take care of this difficulty each cluster has to be symmetrized.

The diagrams related to the entropy: The lowest-order diagram contributing is given by

$$\langle \mathcal{K}_D{}^2 \rangle_{\text{conn}} = (16/4)\langle \sum_{i \neq j} S_i{}^\alpha P_{ij}{}^{\alpha\beta} S_j{}^\beta \sum_{k \neq l} S_k{}^{\alpha'} P_{nl}{}^{\alpha'\beta'} S_l{}^{\beta'} \rangle_c$$

$$= 2 \times 4 \sum_{i \neq j} \langle S_i{}^\alpha S_i{}^{\alpha'} \rangle P_{ij}{}^{\alpha\beta} P_{ij}{}^{\alpha'\beta'} \langle S_j{}^\beta S_j{}^{\beta'} \rangle. \quad (4.2)$$

The factor 2 which we will call the abundance stems from the fact that both $i=k$ with $j=l$ and $i=l$ with

$j=k$ lead to a nonzero result. We have

$$\langle S_i{}^\alpha S_i{}^{\alpha'} \rangle = (\text{Tr} S_i{}^\alpha S_i{}^{\alpha'})/\text{Tr} 1 = \tfrac{1}{4}\delta_{\alpha\alpha'}.$$

Hence

$$\langle \mathcal{K}_D{}^2 \rangle = \tfrac{1}{2} \sum_{i \neq j} (P_{ij}{}^{\alpha\beta})^2$$

$$= N \sum_j [(P_{0j}{}^{xx})^2 + 2(P_{0j}{}^{xy})^2 + (P_{0j}{}^{yy})^2]$$

(for $g_{11}=0$). Note that both i, j, and j, i should be counted in this notation.

In general, a ring diagram of order n is a non-self-crossing loop of n steps. The abundance of such a diagram is $2^{n-1}(n-1)!$ The resulting form for the

FIG. 2. (a) Elements to construct the susceptibility diagrams. (b) Cancellation of diagrams that have articulation points with odd vertices.

entropy is

$$\sigma_{\text{ring}} = \frac{1}{N} \sum_{n=2}^{\infty} (-1)^{n+1} \frac{n-1}{2n} \beta^n P_{n,r}, \qquad (4.3)$$

where

$$P_{n,r} = \sum_{i,j,l,\ldots,t} P_{ij}{}^{\alpha\beta} P_{jl}{}^{\beta\gamma} \cdots P_{ti}{}^{\epsilon\alpha}, \qquad (4.4)$$

where $i,j,l,\ldots,t$ are all different. The actual computation of these ring diagrams will be discussed in Sec. V.

We indicated in Fig. 1(a) all diagrams with six or less vertices. Besides the ring diagram there is an ever increasing number of nonring diagrams, which are ordered according to decreasing number of bonds. Further ordering is arbitrary. The contributions of the fourth- and fifth-order diagrams to the susceptibility are given in Appendix B.

The diagrams related to the susceptibility. One can choose a local coordinate system such that the g tensor is on principal axes. In Garnets and Tutton salts one needs an additional transformation, from local to crystal system, but in CMN the local axes are universal and can be taken along the crystal axes.

As mentioned before the nth-order term in the susceptibility series contains $(n-2)$ dipole-dipole operators $\mathfrak{IC}_D$, and two Zeeman operators $\mathfrak{IC}_z$. For these diagrams we need Zeeman bonds as well as interaction bonds. The heads of the Zeeman bonds remain free (representing a "connection to the magnetic field," and not to a lattice site); they will be represented by an X. Thus, diagram (2-1) of Fig. 1(b) has an "abundance" of unity and gives

$$\langle \mathfrak{IC}_z{}^2 \rangle = H^{\alpha} H^{\beta} \sum_p \mu_p{}^{\alpha} \mu_p{}^{\beta}.$$

Before we proceed with the evaluation of diagram (3-2), we write out $\mathfrak{IC}^3$ and use the cyclic property of the trace operation to find that

$$\mathfrak{IC}^3 = (\mathfrak{IC}_D + \mathfrak{IC}_z)^3 = 3\mathfrak{IC}_D \mathfrak{IC}_z{}^2$$
$$+ \text{(terms not involving } H^2). \quad (4.5)$$

The abundance of this diagram is 2 because end-p can be tied onto end-j, while end-q must be fastened to the one remaining free end in either event. (Compare Fig. 2(a)). However, the 2 is cancelled by the $\frac{1}{2}$ which comes from the summation convention in Eq. (3.6b), and therefore

$$\mathfrak{IC}^3 = 3 \times 2 H^{\alpha} H^{\beta} \sum_{i,j}' P_{ij}{}^{\alpha\beta} \mu_i{}^{\alpha} \mu_j{}^{\beta}$$
$$+ \text{(terms not involving } H^2).$$

The susceptibility is, then, to second order in β,

$$\chi^{\alpha\beta} = \frac{1}{2}\beta \sum_i \mu_i{}^{\alpha} \mu_i{}^{\beta} - \frac{1}{2}\beta^2 \sum_{i,j} P_{ij}{}^{\alpha\beta} \mu_i{}^{\alpha} \mu_j{}^{\beta} + \cdots. \quad (4.6)$$

From this point on, each succeeding term in the series for the chain diagram can be written down immediately. The general term contains the factor

$$P_{n,c} = \sum_{i,j,l,\ldots,t} P_{ij}{}^{\alpha\beta} P_{il}...{}^{\beta\gamma} P_{st}{}^{\epsilon\delta} \mu_i{}^{\alpha} \mu_t{}^{\delta}, \qquad (4.7)$$

where $i,j,l,\ldots,t$ are all different. The contributions of the remaining fifth-order diagrams to $\chi^{\alpha\beta}$ are listed in Appendix A.

V. LATTICE SUMS

A. Fourier Transforms of Ring Diagrams

For each diagram one has to calculate the lattice sum which is most conveniently done by a computer. The number of kinds of lattice summations is actually less than the number of diagrams, since the summations belonging to diagrams with articulation points can be derived from the lattice sums of the nonarticulated diagrams.

Despite the speed of the computer, the number, n, of vertices one can sum is rather limited since each requires three cycles of DO loops and for a radius of, say, 10, this is about 10^{3n} operations. Hence it is more efficient to consider Fourier transforms, in particular for the ring diagrams, as well as for the chain diagrams.

By way of illustration, we first examine P_3 the third-order term in the entropy series for the ring diagrams. It is defined as follows in Eq. (4.4):

$$P_3 = \sum_{i,j,l} P_{ij}{}^{\alpha\beta} P_{jl}{}^{\beta\gamma} P_{li}{}^{\gamma\alpha}. \qquad (5.1)$$

The next step is to transform to a representation in k space by writing the following Fourier series:

$$P^{\alpha\beta}(\mathbf{k}) = \sum_{i,j} P^{\alpha\beta}(\mathbf{r}_{ij}) e^{i\mathbf{k}\cdot\mathbf{r}_{ij}}, \qquad (5.2)$$

where $\mathbf{r}_{ij}$ is the vector from ion i to ion j, that is,

$$\mathbf{r}_{ij} = \mathbf{r}_i - \mathbf{r}_j.$$

Equation (5.2) implies that

$$P^{\alpha\beta}(\mathbf{r}_{ij}) = \frac{1}{V_B} \int_{V_B} P^{\alpha\beta}(\mathbf{k}) e^{-i\mathbf{k}\cdot\mathbf{r}_{ij}} d\mathbf{k}, \qquad (5.3)$$

where V_B is the volume of the first Brillouin zone. It is clear that

$$P^{\alpha\beta}(\mathbf{k}+\mathbf{k}_s)=P^{\alpha\beta}(\mathbf{k}),$$

where $\mathbf{k}_s$ is a reciprocal lattice vector.

At this point it becomes necessary to rewrite Eq. (5.1) in a slightly different form. First, we choose the ith ion as the origin of our coordinate system; second, remove the restrictions on the lattice sum by adding and subtracting the terms with $i=j$, so that

$$P_3=N\sum_{i,j}P_{ij}{}^{\alpha\beta}P_{jl}{}^{\beta\gamma}P_{li}{}^{\gamma\alpha}-N\sum_i P_{ii}{}^{\alpha\beta}P_{il}{}^{\beta\gamma}P_{li}{}^{\gamma\alpha}. \quad (5.4)$$

The last term is identically zero. After substituting Eq. (5.2) into Eq. (5.4) we make use of the relation

$$\sum_m e^{i(\mathbf{k}-\mathbf{k}'')\cdot\mathbf{R}_m}=\frac{(2\pi)^3}{\Omega}\delta(\mathbf{k}-\mathbf{k}'') \quad (5.5)$$

to argue that

$$P_3=\frac{N\Omega}{(2\pi)^3}\int_{V_B} P^{\alpha\beta}(\mathbf{k})P^{\beta\gamma}(\mathbf{k})P^{\gamma\alpha}(\mathbf{k})d\mathbf{k}, \quad (5.6)$$

where Ω is the volume of the unit cell in real space. If we follow the same procedure in evaluating P_4 the result is

$$P_4=\frac{N\Omega}{(2\pi)^3}\int_{V_B} P^{\alpha\beta}(\mathbf{k})P^{\beta\gamma}(\mathbf{k})P^{\gamma\delta}(\mathbf{k})P^{\delta\alpha}(\mathbf{k})d\mathbf{k}$$
$$-2N\sum_{i,k}P_{ij}{}^{\beta\alpha}P_{ij}{}^{\alpha\delta}P_{jk}{}^{\delta\gamma}P_{jk}{}^{\gamma\beta}. \quad (5.7)$$

The last term in Eq. (5.7) results from the removal of the restrictions on the lattice summations, and it adds to the expression for $\Delta S/NK$ an amount equal to

$$\frac{3}{4(KT)^4}\sum_{i,k}P_{ij}{}^{\alpha\beta}P_{ij}{}^{\alpha\delta}P_{jk}{}^{\delta\gamma}P_{jk}{}^{\gamma\beta}.$$

This term resembles, but is not equal to that represented by diagram (4.3)a of Fig. 1(a) which itself adds to $\Delta S/NK$ the quantity

$$\frac{-3}{4(KT)^4}\sum_{i,k}{}' P_{ij}{}^{\alpha\beta}P_{ij}{}^{\alpha\beta}P_{jk}{}^{\beta\gamma}P_{jk}{}^{\beta\gamma}$$

which becomes

$$\frac{3}{4(KT)^4}\Big[\sum_i P_{ij}{}^{\alpha\beta}P_{ij}{}^{\alpha\beta}P_{ij}{}^{\beta\gamma}P_{ij}{}^{\beta\gamma}$$
$$-\sum_{i,k}P_{ij}{}^{\alpha\beta}P_{ij}{}^{\alpha\beta}P_{jk}{}^{\beta\gamma}P_{jk}{}^{\beta\gamma}\Big].$$

The second term in the above expression is approximately N times as large as the first, since it has one

more summation. Therefore, we will neglect the first term when we combine the result with the last term in Eq. (5.7) to yield

$$\frac{3}{4(KT)^4}\sum_{\alpha,\beta,\gamma,\delta\ \beta\neq\delta}\Big[\sum_{i,k}P_{ij}{}^{\alpha\beta}P_{ij}{}^{\alpha\delta}P_{jk}{}^{\delta\gamma}P_{jk}{}^{\gamma\beta}\Big],$$

which is added to $\Delta S/NK$. In essence, then, the contribution from diagram (4.3)a of Fig. 1 is partially cancelled, as indicated by the loss of the terms with $\delta=\beta$ in the above expression.

B. Nonring Entropy Diagrams

There are a number of nonring diagrams contributing to the entropy. They can be further subdivided in diagrams with and without articulation points. Among the last there are diagrams that contain internal single links, for example (6-5)a in Fig. 1(a). Such diagrams lead to shape-dependent results in the lattice sum as was noticed by Levy,[14] since they contain a partial summation, that is, they are conditionally convergent. Hence it looks at first sight that the specific heat would be slightly shape-dependent. One can show however, that for topological reasons these diagrams do not contribute to the zero-field entropy. The argument is as follows (compare Fig. 3): For each diagram with a "stick," we have a counterpart where the rest of the diagram is reflected. The circles A, B, and B′ represent the rest of the diagram. An example is (6-5)c of Fig. 1. Since we have

$$\mathrm{Tr}(S_\beta S_\alpha S_\gamma)=-\mathrm{Tr}(S_\gamma S_\alpha S_\beta),$$

the net contribution will be zero. If the vertex is not a triangle but a larger odd polygon, the same argument holds. In the case that the vertex-polygon at the end of the "stick" is even, then the situation is slightly more complicated. In such a diagram [take (6-4)b in Fig. 1(d), for example] we find that there is always at least one odd-vertex. In this vertex the circulation can be taken both clockwise and counterclockwise, which leads again to cancellation.

Note that the above arguments are only valid for articulation points. If we deal with odd vertices in multiply connected diagrams such as (3-2) in Fig. 1(a) or (5-2) in Fig. 1(b) the reversal of the cycle will affect both vertices simultaneously and there will be no sign change, hence no cancellation. The fact that the articulation point is at the end of a "stick" is irrelevant; for instance, (5-3)a in Fig. 2 is of the self-cancelling type and so is any articulation point from which emanates an odd number of bonds to one or more pieces of a diagram.

The considerations are general. In CMN we can use a much simpler rule. If $g_{11}=0$ we deal with a two-dimensional spin hence all diagrams with odd vertices are zero, which includes now for instance (3-2).

C. Fourier Transform of Chain Diagram

We will begin by considering the fourth-order chain diagram,

$$D_4 = \tfrac{1}{2}N\left(\sum_{i,j} P_{ij}{}^{\alpha\gamma}P_{jk}{}^{\gamma\beta}\right)\mu^\alpha\mu^\beta \qquad (5.8)$$

if we assume that the g factor is the same for all the cerium ions. Utilizing Eqs. (5.2), (5.5), and (5.8), we find that

$$D_4 = \tfrac{1}{2}N\mu^\alpha\mu^\beta P^{\alpha\gamma}(\mathbf{k}=0)P^{\gamma\beta}(\mathbf{k}=0). \qquad (5.9)$$

Similarly, if we define

$$D_5 = -\tfrac{1}{2}\sum_{i,j,k,l}' P_{ij}{}^{\alpha\gamma}P_{jk}{}^{\gamma\delta}P_{kl}{}^{\delta\beta}\mu_i{}^\alpha\mu_l{}^\beta, \qquad (5.10)$$

we can show that

$$D_5 = -\tfrac{1}{2}N\mu^\alpha\mu^\beta P^{\alpha\gamma}(\mathbf{k}=0)P^{\gamma\delta}(\mathbf{k}=0)P^{\delta\beta}(\mathbf{k}=0)$$

$$+N\mu^\alpha\mu^\beta\sum_{j,l} P_{ij}{}^{\alpha\gamma}P_{ji}{}^{\gamma\delta}P_{il}{}^{\delta\beta}$$

$$+\tfrac{1}{2}N\mu^\alpha\mu^\beta\sum_{j,k} P_{ij}{}^{\alpha\gamma}P_{jk}{}^{\gamma\delta}P_{ki}{}^{\delta\beta}.$$

The last two terms appear in the expression for D_5 as a consequence of resorting to unrestricted summations. For the sake of clarity in what follows we shall label them respectively as D_5' and D_5'':

$$D_5' = N\mu^\alpha\mu^\beta\sum_{j,l} P_{ij}{}^{\alpha\gamma}P_{ij}{}^{\gamma\delta}P_{il}{}^{\delta\beta},$$

$$D_5'' = \tfrac{1}{2}N\mu^\alpha\mu^\beta\sum_{j,k} P_{ij}{}^{\alpha\gamma}P_{jk}{}^{\gamma\delta}P_{ki}{}^{\delta\beta}.$$

These two terms resemble the contributions of diagrams (5-3)a and (5-3)b, respectively, which are given by

$$32N\sum_{j,l}' P_{ij}{}^{\alpha\beta}P_{ij}{}^{\alpha\beta}P_{il}{}^{\alpha\delta}\mu_i{}^\alpha\mu_l{}^\delta \qquad (5.3')$$

and

$$16N\sum_{j,k} P_{ij}{}^{\alpha\beta}P_{jk}{}^{\beta\gamma}P_{ki}{}^{\gamma\alpha}\mu_i{}^\alpha\mu_i{}^\alpha, \qquad (5.3'')$$

and once again making use of unrestricted summations we can write for diagram (5-3)a

$$32N\mu^\alpha\mu^\delta\sum_{j,l} P_{ij}{}^{\alpha\beta}P_{ij}{}^{\alpha\beta}P_{ij}{}^{\alpha\delta}$$

$$-32N\mu^\alpha\mu^\delta\sum_{j} P_{ij}{}^{\alpha\beta}P_{ij}{}^{\alpha\beta}P_{ij}{}^{\alpha\delta}, \qquad (5.3')$$

where the second term can be neglected, since it is of the order $1/N$ of the first term, which in turn partially cancels D_5', leaving

$$-32N\sum_{\alpha,\beta,\gamma,\delta\ \gamma\neq\alpha}\left(\mu^\alpha\mu^\delta\sum_{j,l} P_{ij}{}^{\alpha\beta}P_{ij}{}^{\gamma\beta}P_{il}{}^{\gamma\delta}\right).$$

Similarly, (5-3)b and D_5'' combine to yield

$$-16N\sum_{\alpha,\beta,\gamma,\delta\ \delta\neq\alpha}\left(\mu^\alpha\mu^\delta\sum_{j,k} P_{ij}{}^{\alpha\beta}P_{jk}{}^{\beta\gamma}P_{ki}{}^{\gamma\delta}\right).$$

D. Tensor Summation

Finally, one is faced with a multiple summation over the Greek indices, which describe the tensorial character of the interaction. [Compare Eqs. (4.4) and (4.7).] This step is greatly simplified by a procedure originally introduced by Kramers and Wannier.[15] Consider $P^{\alpha\beta}(k)$ as a 3×3 matrix; this is

$$\mathbf{P}(\mathbf{k}) = \begin{bmatrix} P^{xx}(\mathbf{k}) & P^{xy}(\mathbf{k}) & P^{xz}(\mathbf{k}) \\ P^{yx}(\mathbf{k}) & P^{yy}(\mathbf{k}) & P^{yz}(\mathbf{k}) \\ P^{zx}(\mathbf{k}) & P^{zy}(\mathbf{k}) & P^{zz}(\mathbf{k}) \end{bmatrix}. \qquad (5.11)$$

These summations can then be interpreted as matrix multiplications, and

$$\sum_{\alpha,\beta,\gamma,\delta} P^{\alpha\beta}(\mathbf{k})P^{\beta\gamma}(\mathbf{k})\cdots P^{\delta\alpha}(\mathbf{k})$$

$$= \mathrm{Tr}[P^{\alpha\beta}(\mathbf{k})P^{\beta\gamma}(\mathbf{k})\cdots P^{\delta\alpha}(\mathbf{k})]$$

$$= \mathrm{Tr}\begin{bmatrix} \lambda_1{}^n & 0 & 0 \\ 0 & \lambda_2{}^n & 0 \\ 0 & 0 & \lambda_3{}^n \end{bmatrix} = \sum_{i=1}^{3} \lambda_i{}^n(\mathbf{k}), \qquad (5.12)$$

where there are n of the $\mathbf{P}(\mathbf{k})$ matrices under the summation. The λ's are the diagonal elements of the matrix $P^{\alpha\beta}(\mathbf{k})$ so we can rewrite Eq. (5.6) as follows:

$$P_3 = \frac{N\Omega}{(2\pi)^3}\int_{V_B} [\lambda_1{}^3(\mathbf{k})+\lambda_2{}^3(\mathbf{k})+\lambda_3{}^3(\mathbf{k})]d\mathbf{k}. \qquad (5.13)$$

We shall defer the explicit calculation of the λ's until a later section and now attempt to apply the prescription of Kramers and Wannier to a calculation of the susceptibility as represented by the chain diagrams. A glance at Eq. (4.7), (5.8), and (5.11) will reveal that the $(n+2)$th order contribution to the susceptibility, denoted $\chi_{n+2}{}^{\alpha\beta}$, can be expressed proportionately as

$$\chi_{n+2}{}^{\alpha\beta} \approx \sum_{\alpha,\gamma\ \delta,\rho,\beta} \mu^\alpha\mu^\beta P^{\alpha\gamma}(\mathbf{k}=0)$$

$$\times P^{\gamma\delta}(\mathbf{k}=0)\cdots P^{\rho\beta}(\mathbf{k}=0). \qquad (5.14)$$

Suppose that $\mathbf{B}$ is the orthogonal transformation that diagonalizes $\mathbf{P}$, i.e.,

$$\lambda = \mathbf{B}^{-1}\mathbf{P}_0\mathbf{B},$$

where $\mathbf{P}_0$ represents the 3×3 matrix, $\mathbf{P}^{\alpha\beta}(\mathbf{k}=0)$ and

$$\lambda(0) = \begin{bmatrix} \lambda_1 & 0 & 0 \\ 0 & \lambda_2 & 0 \\ 0 & 0 & \lambda_3 \end{bmatrix}.$$

Proportionality (5.14) is then more simply expressed as

$$\chi_{n+2} \approx \mu\mu\mathbf{P}_0\mathbf{P}_0\cdots\mathbf{P}_0$$

$$= \mu\mu\mathbf{B}[\lambda(0)]^n\mathbf{B}^{-1}. \qquad (5.15)$$

[15] H. A. Kramers and G. H. Wannier, Phys. Rev. 60, 252 (1957).

Therefore, we find the following series representing

$$\chi = \tfrac{1}{2} N \boldsymbol{\mu}\boldsymbol{\mu} \beta \sum_{n=0}^{\infty} (-\beta)^n \mathbf{B} [\lambda(0)]^n \mathbf{B}^{-1}. \qquad (5.16)$$

Once $\lambda(0)$ and $\mathbf{B}$ are determined, one could then inspect each component of χ for possible singularities. It is more than likely that the component with the highest singular temperature T_c will determine the direction of the magnetization as well as the critical temperature. Below this temperature the moment method is no longer valid.

It is generally assumed that the singularities in the specific heat and the susceptibility coincide. Hence, a knowledge of the specific-heat singularity (as found from the entropy series) can be of assistance in determining the behavior of the susceptibility just above the critical temperature.

E. Susceptibility in a Nonuniform Magnetic Field

Up to this point we have only considered the case of a uniform magnetic field $\mathbf{H}$ acting on each magnetic ion. It would be instructive to insert into the Hamiltonian a nonuniform field $\mathbf{H}(\mathbf{r})$ given by

$$H^\tau(\mathbf{r}) = \sum_{\mathbf{g}} H_{\mathbf{g}}^\tau e^{i\mathbf{g}\cdot\mathbf{r}}, \quad \tau = x,y,z \qquad (5.17)$$

where $\mathbf{g}$ is an arbitrary wave vector and $H^\tau(\mathbf{r})$ is periodic with an as yet unspecified periodicity. If the only nonvanishing $H_{\mathbf{g}}^\tau$, in Eq. (5.18) were H_0^τ we should have a uniform field, which has occupied our attention to this point. We would emphasize the point that Eq. (5.18) allows for the possibility of antiferromagnetic behavior below the transition temperature using a staggered field, whereas the assumption that only a uniform field is acting precludes any investigation of the susceptibility not associated with the ferromagnetic state.

The pattern linked with antiferromagnetism is given by Eq. (5.1) with three equal nonzero wave vectors:

$$\mathbf{g}_1 = (\pi/a,0,0), \quad \mathbf{g}_2 = (0,\pi/a,0), \quad \mathbf{g}_3 = (0,0,\pi/a).$$

It is evident that such an arrangement can only occur in a cubic lattice.

If we imagine a "staggered field," of periodicity $\mathbf{g}$ acting on the sample, then Eq. (5.18) reduces to

$$H^\tau(\mathbf{r}) = H_{\mathbf{g}}^\tau e^{i\mathbf{g}\cdot\mathbf{r}}. \qquad (5.18)$$

To find the susceptibility for the chain diagrams under these conditions we return to the previous section. There is one significant difference: If the ends of the chain are labeled i and k, then both $H_{\mathbf{g}}^\tau(\mathbf{r}_i)$ and $H_{\mathbf{g}}^\tau(\mathbf{r}_k)$ explicitly enter the calculation at the outset. The rest of the calculation proceeds as before with the result that

$$\chi = \frac{N\boldsymbol{\mu}:\boldsymbol{\mu}}{2KT} \mathbf{B} \left[\frac{1}{1+\beta\lambda(\mathbf{g})} \right] \mathbf{B}^{-1}. \qquad (5.19)$$
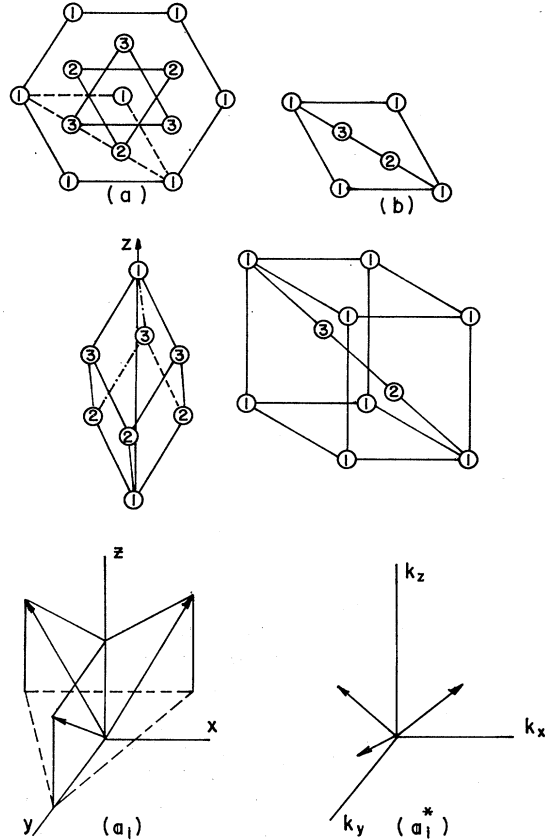

FIG. 3. (a) and (b) projected view of unit cell in two different representations; (c) and (d) same in three-dimensional form. (e) and (f) primitive vectors in the crystal and in k space.

VI. PARAMETERS ASSOCIATED WITH CMN

The crystal structure of CMN is trigonal. Only the cerium atoms need be considered as they are the sole carriers of a magnetic moment, and so the lattice can be described as follows: Imagine three sets of parallel planes at $z=0$, $\tfrac{1}{3}c$, and $\tfrac{2}{3}c$, each containing a triangular array of atoms separated by a distance a. The relative orientation is given in Figs. 3(a) and 3(b). An alternative way to view this structure is shown in Figs. 3(c) and

TABLE I. Influence of c/a ratio on the lattice sums with $F(r/R) = 1$.

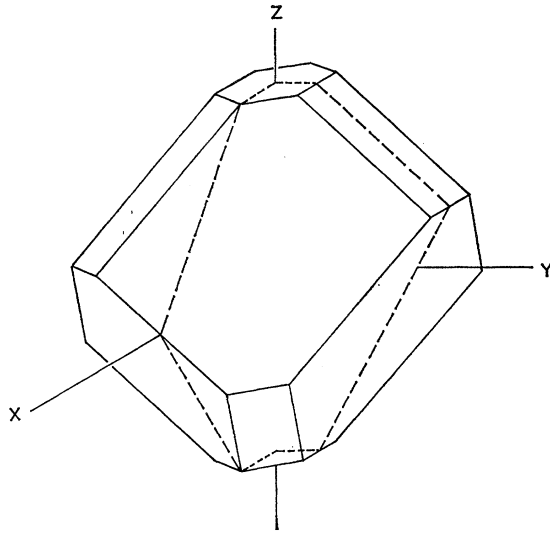| c/a	1.73	1.57	1.41	1.225	Radius
P^{xx}	0.72	0.70	0.49	0	10.5
P^{yy}	0.72	0.70	0.49	0	10.5
P^{xy}	0	0	0	0	10.5
$(P^{xx})^2$	19.08	22.84	28.70	40.49	10.5
$(P^{yy})^2$	19.08	22.84	28.70	40.49	10.5
$(P^{xy})^2$	15.15	18.94	24.73	35.90	10.5
$(P^{xx})^3$	49.89	56.18	59.60	65.65	3.0
$P^{xx}(P^{xy})^2$	44.82	56.29	69.25	82.18	3.0
$P^{yy}(P^{xy})^2$	4.15	1.58	−2.45	−3.22	3.0
$(P^{yy})^3$	90.56	110.88	131.3	151.0	3.0

FIG. 4. Brillouin zone for CMN in actual proportions.

4(a). Figure 3(a) represents one atom per unit cell, inasmuch as each corner is shared by eight cells, and further corresponds to a cube that is elongated along the body diagonal. The actual value of c/a used in the calculations was 1.572 with a being equal to 11.004 Å.[16] Ratios 10% above and below 1.572 were also utilized to study the influence of a lattice contraction or expansion, and the results can be seen in Table I. If the lattice were cubic, there would be no contribution to the dipole lattice sum for the usual spherical boundary, as is well known from the Lorentz theory.[3] This fact can be and was used as a test for the numerical calculations on the computer. The results are in Table I, the next to the last column. If we assume that the nondipolar interaction between spins is indeed small, and there are experiments to confirm this, one could conceivably improve the crystal, from the thermometric point of view, by introducing a mechanical deformation to make the crystal more cubic, thereby lowering the critical temperature.

The choice of primitive lattice vectors a_i is given in Figs. 3(e) and 3(f) along with $a_i{}^*$, the resulting primitive lattice vectors in k space. If we use units such that $a=1$ (therefore c means c/a), the expressions are

$$a_1 = \begin{bmatrix} \frac{1}{2} \\ 1/2\sqrt{3} \\ \frac{1}{3}c \end{bmatrix}, \quad a_2 = \begin{bmatrix} -\frac{1}{2} \\ 1/2\sqrt{3} \\ \frac{1}{3}c \end{bmatrix}, \quad a_3 = \begin{bmatrix} 0 \\ -1/\sqrt{3} \\ \frac{1}{3}c \end{bmatrix};$$

and

$$a_1{}^* = \begin{bmatrix} 1 \\ 1/\sqrt{3} \\ 1/c \end{bmatrix}, \quad a_2{}^* = \begin{bmatrix} -1 \\ 1/\sqrt{3} \\ 1/c \end{bmatrix}, \quad a_3{}^* = \begin{bmatrix} 0 \\ -2/\sqrt{3} \\ 1/c \end{bmatrix}.$$

The YOZ plane and the XOY planes are reflection planes, and there is, of course, a threefold rotation possible around the z axis. The resulting Brillouin zone

[16] A. Zalkin, J. D. Forrester, and D. H. Templeton, J. Chem. Phys. **39**, 2881 (1963).

was constructed algebraically by looking for sets of integers n_i that fulfill the conditions

$$2\mathbf{k} \cdot \mathbf{G} + G^2 = 0, \quad \mathbf{G} = 2\pi(n_1 a_1{}^* + n_2 a_2{}^* + n_3 a_3{}^*)$$

for the vectors $\mathbf{G}$ closest to the origin. In general, there are two possible types of Brillouin zones for the trigonal structure depending on the "openness of the cone" formed by the three primitive lattice vectors. In one zone the cone is more "open" than a cube; in the other it is more closed than a cube. For our case the primitive lattice vectors are more closed than a cube, hence the inverse lattice vectors are more open and we obtain a Brillouin zone of the "flat-top" type.[17] However, the c/a ratio is not that much different from a cube, so the figure was drawn to scale to show the actual shape of the zone in Fig. 4.

Because of symmetry, it is only necessary to calculate the integers, n_i, for those faces in the octants $k_x > 0$, $k_y > 0$, $k_z \lessgtr 0$, and these faces correspond to the following equations (using $c/a = 1.577$):

$$2k_y/\sqrt{3} - k_z/c = 5.452, \tag{6.1}$$

$$k_x + k_y/\sqrt{3} + k_z/c = 5.452, \tag{6.2}$$

$$2k_y/\sqrt{3} + 2k_z/c = 9.242, \tag{6.3}$$

$$k_x - k_y/\sqrt{3} - k_z/c = 5.452, \tag{6.4}$$

$$k_x + k_y/\sqrt{3} - 2k_z/c = 9.242, \tag{6.5}$$

$$k_z = 5.977, \tag{6.6}$$

$$k_z = -5.977. \tag{6.7}$$

The corresponding Miller indices are found in Table II. One final parameter associated with CMN is needed for the calculations. It is the g tensor which has been measured by Cooke, Duffus and Wolf.[18] They give a value of $g_\perp = 1.84$ and $g_{||} \leqslant 0.1$. As a result, the matrix $\mathbf{P}(\mathbf{k})$ can be diagonalized explicitly in accordance with Eq. (5.12) to yield

$$\lambda(\mathbf{k})_{1,2} = \tfrac{1}{2}[P^{xx}(\mathbf{k}) + P^{yy}(\mathbf{k})]$$
$$\pm \{\tfrac{1}{4}[P^{xx}(\mathbf{k}) - P^{yy}(\mathbf{k})]^2 + [P^{xy}(\mathbf{k})]^2\}^{1/2},$$
$$\lambda(\mathbf{k})_3 = 0.$$

Our program used initially this formula, but was later revised to do the three by three diagonalization. This was done to study the influence of a small $g_{||}$, which is of no importance as was shown in Ref. 7, but also to be prepared to handle other compounds besides CMN in the future.

VII. CALCULATIONS AND CONCLUSIONS

A. Lattice Sum Computer Program

The computer programs were written in FORTRAN IV, and all the lattice sums calculated were expressed in

[17] G. F. Koster, in *Solid State Physics*, edited by F. Seitz and D. Turnbull (Academic, New York, 1957), Vol. 5.
[18] A. H. Cooke, J. H. Duffus, and W. P. Wolf, Phil. Mag. **44**, 623 (1953).

TABLE II. The corresponding Miller indices.

n_i \ Eq.	(5.1)	(5.2)	(5.3)	(5.4)	(5.5)	(5.6)	(5.7)
n_1	0	−1	−1	0	0	−1	1
n_2	0	0	−1	1	1	−1	1
n_3	1	0	0	0	1	−1	1

dimensionless units by taking the unit of length equal to the lattice constant a. It must also be noted that henceforth all lattice summations referred to make use of a symbol $P_{ij}^{\alpha\beta}$ which does not include the constants μ_β and $g^{\alpha\beta}$ anymore. [See Eq. (7.1).] The first lattice sums computed were the following:

$$\sum_i P_{ij}^{xx}, \quad \sum_i P_{ij}^{xy}, \quad \sum_i P_{ij}^{yy},$$

$$\sum_i P_{ij}^{xx}P_{ij}^{xx}, \quad \sum_i P_{ij}^{xy}P_{ij}^{xy}, \quad \sum_i P_{ij}^{yy}P_{ij}^{yy},$$

where the sums were taken over all values of i for a fixed j, which meant that the origin of the coordinate system was at the jth ion. The calculations were done by summing the contributions to each lattice sum over successive spherical shells where R, the radius of the outermost shell, was some arbitrary multiple of a. The problem of convergence of $\sum P^{xx}$ and $\sum P^{yy}$ arises inasmuch as each of these sums is equal to the difference of two separately divergent sums. For instance,

$$\sum_i P_{ij}^{xx} = \sum_i \frac{1}{r_{ij}^3} - 3\sum_i \frac{x_{ij}^2}{r_{ij}^5}. \quad (7.1)$$

It is well known (cf. References 6 and 19) that, for large values of R, the contribution of each shell to $\sum P^{xx}$ or to $\sum P^{yy}$ can be replaced by an integral over the shell and, further, that this integral is equal to zero. Therefore to insure convergence one only needs to have the lattice sums taken over a sphere so large that the contribution of the next shell be negligible (see Appendix B). In actual practice, however, $F(r/R)$, the weighting function of Peverley and Meijer,[19] was utilized in the

TABLE III. Influence of the function $F(r/R)$ on first-order lattice sums with $c/a = 1.577$.

F	R Outer radius	$\sum_i P_{ij}^{\alpha\beta}$ P^{xx}	P^{yy}	P^{xy}
1	5	0.6698	0.6698	0
1	5.5	0.8308	0.8308	0
1	10	0.6804	0.6803	0
1	10.5	0.6874	0.6873	0
≠1	5	0.6883	0.6883	0
≠1	5.5	0.6913	0.6912	0

[19] J. R. Peverley and P. H. E. Meijer, Phys. Status Solidi **23**, 353 (1967).

TABLE IV. Influence of the function $F(r/R)$ on second-order lattice sums with $c/a = 1.577$.

F	R Outer radius	$\sum_i (P_{ij}^{\alpha\beta})^2$ $(P^{xx})^2$	$(P^{yy})^2$	$(P^{xy})^2$
1	5	22.64	22.64	18.75
1	5.5	22.65	22.65	18.76
1	10.0	22.69	22.69	18.79
1	10.5	22.69	22.69	18.79
≠1	5	22.56	22.56	18.69
≠1	5.5	22.59	22.59	18.71

early calculations. This function is of the form

$$F\left(\frac{r}{R}\right) = \frac{1}{\exp[A(Br^2/R^2 - 1)] + 1}, \quad (7.2)$$

where A and B are adjustable parameters. Peverley and Meijer demonstrated by their computations that a modified sum,

$$\sum_i \left[\left(\frac{3z_{ij}^2 - r_{ij}^2}{r_{ij}^5} \right) F\left(\frac{r_{ij}}{R} \right) \right] \quad r_{ij} < R$$

did converge to the same limit as the sum without $F(r/R)$ and indeed did so at a faster rate. Our calculations seem to indicate that the limits were essentially the same. This is illustrated in Table III. The effect of the weighting function is not as pronounced in Table IV, for it appears that $\sum P^2$ converges better than $\sum P$. In Table V we tabulated some results for the lattice sum of diagram (3-3) in Fig. 1 and various combinations of different weighting factors were tried. By way of explanation $F1$ is defined by Eq. (7.2) with r_i substituted for r, $F2$ has r_j, and $F3$ uses r_{ij} for r. No conclusions concerning the effect of the weight factors can be drawn from this table and in any event the length of computer time for this lattice summation became prohibitive so it was pursued no further. However, the results shown in Table V did more or less corroborate the assumption made in Sec. III that the lattice sum for Diagram (3-3) would give a contribution of the order of N times as large as diagram (3-2) in Fig. 1. With all the weighting

TABLE V. Influence of the function $F(r/R)$ on third-order lattice sums with $c/a = 1.577$.

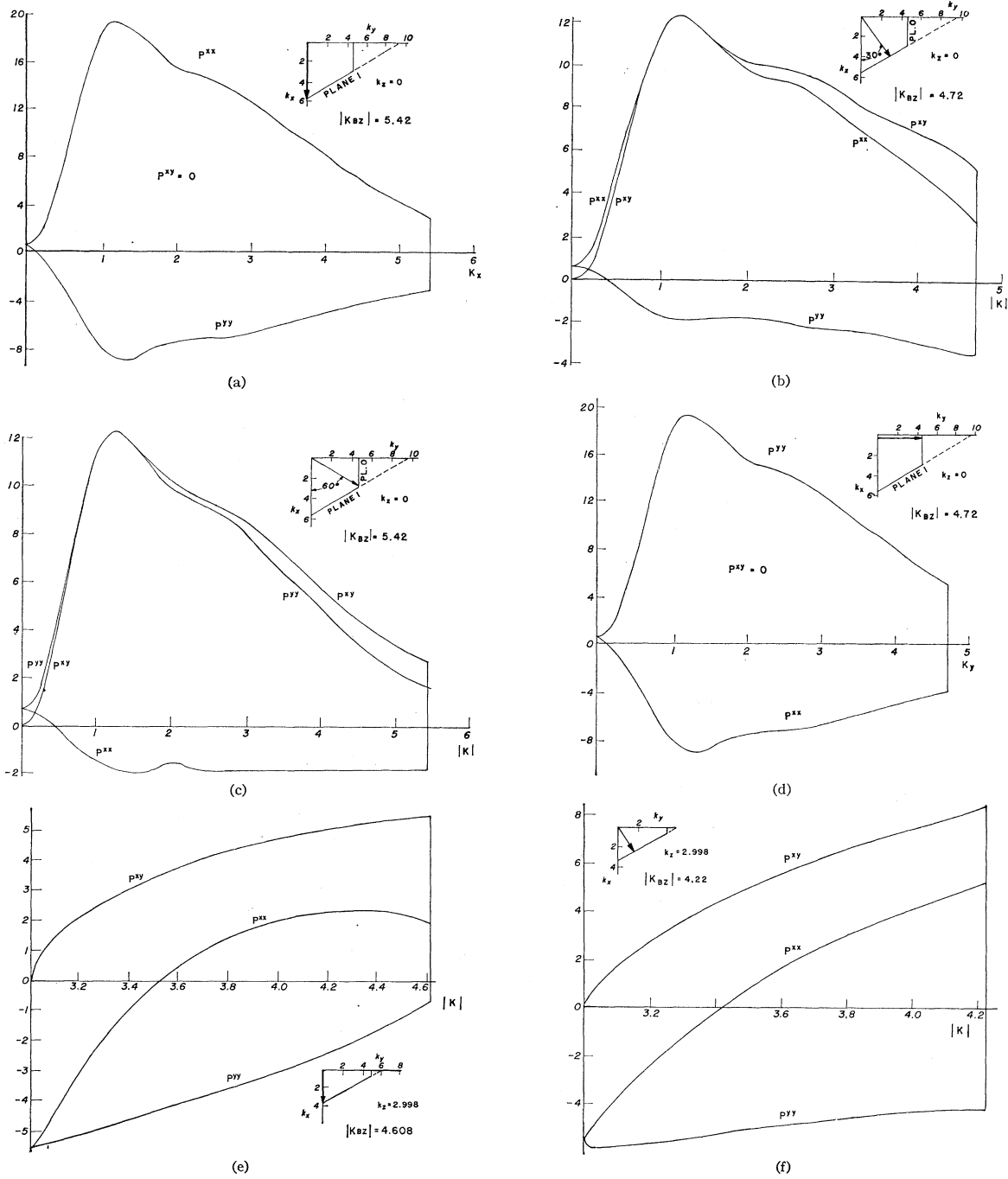| F's	R Outer radius	$\sum_{i,j}' P_{ij}^{\alpha\beta} P_{jl}^{\beta\gamma} P_{li}^{\gamma\alpha}$ $(P^{xx})^3$	$(P^{yy})^3$	$P^{xx}(P^{xy})^2$	$P^{yy}(P^{xy})^2$
all in	3.0	54.22	107.8	54.82	1.261
all in	3.5	55.89	109.7	55.57	1.748
all in	4.0	56.86	110.6	55.82	2.114
$F3 = 1$	5.0	57.68	111.4	56.11	2.388
$F2 = 1$ $F3 = 1$	5.0	57.86	111.6	56.19	2.433

FIG. 5. Fourier transform of the lattice sum for various directions in k space, from the origin to the zone boundary. Inserts indicate the direction chosen. The g factors are not incorpoarted in the sum. Units are $a=1$ and $c/a=1.572$.

functions equal to unity and $R=10.5$, we found

$$\sum_i (P_{ij}{}^{xx})^3 = 2.347,$$

$$\sum_i (P_{ij}{}^{yy})^3 = -3.5708,$$

$$\sum_i (P_{ij}{}^{xy})^3 = 0$$

whereas the values in Table V are at least an order of magnitude greater. It must be pointed out that the c/a ratio for Tables III–VI was 1.577, while Table I depicts the influence of the c/a ratio on the lattice summations, while the remaining tables use a value of 1.572 for c/a. In Table VI we can note the following. First of all the use of double precision in the computer program was not
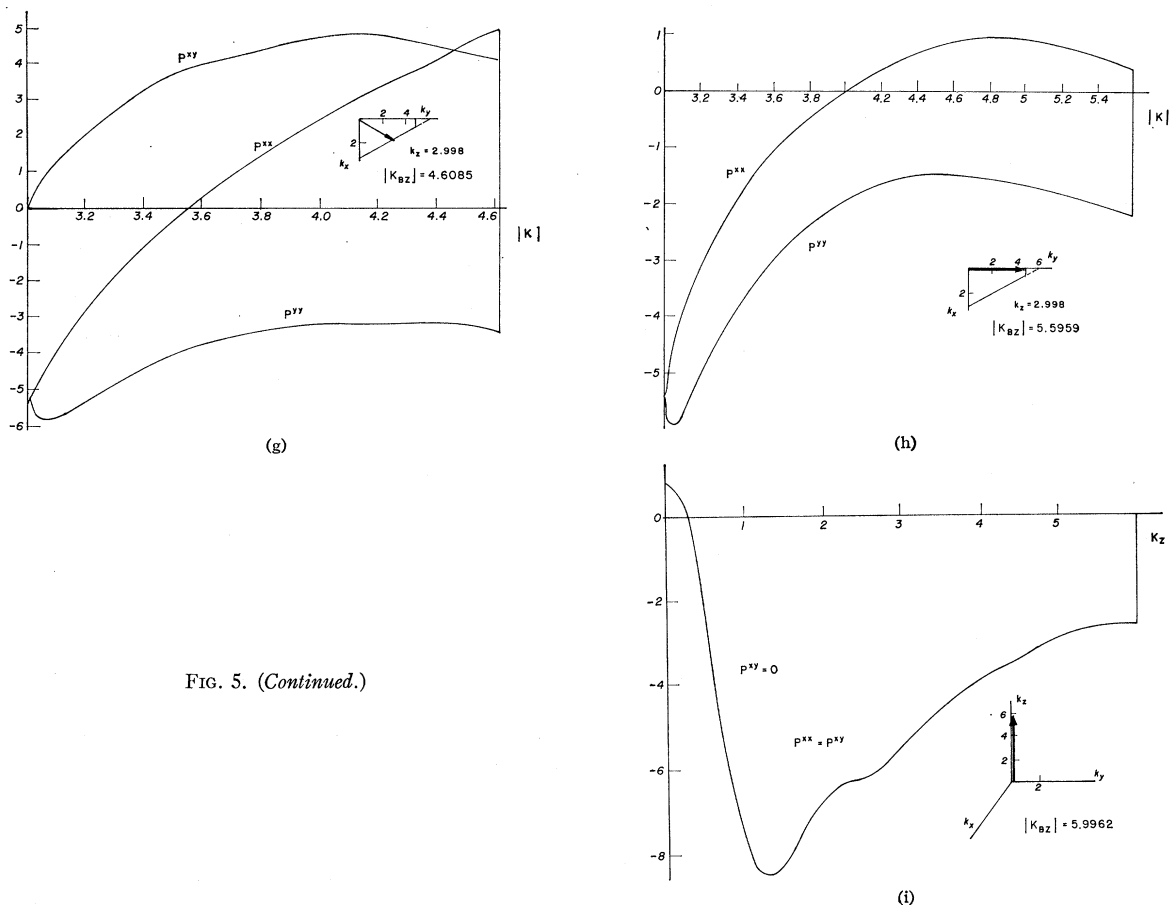
(g)

(h)

(i)

FIG. 5. (Continued.)

justified for the first- and second-order terms. Secondly, good convergence is attained at $R=11.0$ for $\sum P$, since the sum for $R=12.0$ is not even 1% greater. Finally, it is again evident that $\sum P^2$ converges faster than $\sum P$.

The last table dealing with the direct lattice summations is Table VII and in this case better than 1% convergence in the entropy is evident at a radius of 4. It was necessary to resort to double precision for these lattice sums, for without it the last two columns were unequal, and of course, this cannot be.

B. Fourier Transform Program

A modified lattice sum program furnished $P^{\alpha\beta}(\mathbf{k})$ for various values of $\mathbf{k}$. [See Figs. 5(a)–5(i)]. The next step was to effect the solution of Eq. (5.14) by a relatively coarse integration over the first Brillouin zone. The procedure was to calculate, for example, $P^{xx}(\mathbf{k})^3$ for some known value of $\mathbf{k}$ and multiply it by an element of volume in k space, and then sum these products over the Brillouin zone. Equations (6.1)–(6.7) were used to test whether the value of $\mathbf{k}$ was inside or outside the zone. In order to save computer time the final runs were done without the Brillouin zone, but with a parallelepiped of equal volume whose edges were the reciprocal-lattice vectors $\mathbf{a}_i^*$. The results are given in Table VIII

TABLE VI. First- and second-order lattice sums with $c/a = 1.5718$ and $F(r/R) = 1$.

(A) $\sum_i P_{ij}{}^{\alpha\beta}$

Precision	R Outer radius	P^{xx}	P^{yy}	P^{xy}
Single	10.0	0.67186	0.67780	0
Single	10.5	0.69484	0.69485	0
Single	11.0	0.68696	0.69137	0
Single	11.5	0.69101	0.69099	0
Double	10.0	0.67215	0.67814	0
Double	10.5	0.69519	0.69518	0
Double	11.0	0.68732	0.69183	0
Double	12.0	0.68282	0.68630	0
Double	13.0	0.68796	0.69069	0
Double	14.0	0.68638	0.68856	0

(B) $\sum_i (P_{ij}{}^{\alpha\beta})^2$

		$(P^{xx})^2$	$(P^{yy})^2$	$(P^{xy})^2$
Single	10.0	22.824	22.825	18.924
Single	10.5	22.825	22.826	18.924
Single	11.0	22.825	22.826	18.924
Single	11.5	22.825	22.826	18.925
Double	10.0	22.840	22.840	18.936
Double	10.5	22.841	22.841	18.937
Double	11.0	22.842	22.842	18.938
Double	12.0	22.843	22.843	18.939
Double	13.0	22.844	22.844	18.939
Double	14.0	22.845	22.845	18.940

TABLE VII. Third-order entropy correction and lattice sums in double precision with $c/a=1,5718$ and $F(r/R)=1$.

Entropy correction (10^{-9})	R Outer radius	$\sum(P^{xx})^3$	$\sum(P^{yy})^3$	$\sum(P^{xy})^2 P^{yy}$	$\sum P^{xy}P^{xx}P^{xy}$	$\sum P^{xx}P^{xy}P^{xy}$
6.7837	3	56.2192	110.804	1.8509	56.1377	56.1377
6.9020	4	58.0373	112.184	2.4083	56.4974	56.4974
6.9367	5	58.4352	112.677	2.4819	56.7078	56.7078

for different radii, different numbers of points in k space, with and without double precision. The best results obtained are displayed in Table IX. The first column is the number of bonds n; the second and third are the Fourier integrals of both eigenvalues:

$$I_i = \frac{\Omega}{(2\pi)^3}\int \lambda_i^n d\mathbf{k}, \quad i=1,2.$$

The last column is the combined result for the coefficients of T^{-n} in the entropy expansion, with T expressed in mK. For testing, $n=1$ is also computed. Only for $n=2,3$ has the direct lattice sum been determined. The c/a ratio equals 1.5718 and VE, the volume element in k space, equals $\Delta k_x \Delta k_y \Delta k_z$, where

$$I_i = \frac{c}{2(2\pi)^3 3}\sum_{k\ ip} \lambda_i^n \Delta k_x \Delta k_y \Delta k_z, \quad i=1,2$$

where ip denotes inside parallelepiped.

The convergence of the Fourier transform of the lattice sum is due to two entirely different processes. One dominates in the region of small k and the other in the region of large k. In the region of small k the convergence is only conditional. In the region of large k the

TABLE VIII. $\Delta S2$ and $\Delta S3$, the second- and third-order entropy contributions from the Fourier integrals of the ring diagrams, with $c/a=1.5718$.

$\Delta S2$ (10^{-6})	R Outer radius	No. of points in parallel-epiped	$\int(\lambda+\mu)\,d\mathbf{k}$ over parallel-epiped	$\int(\lambda^2+\mu^2)\,d\mathbf{k}$ over parallel-epiped	$\Delta S3$ (10^{-9})
(A) Single Precision					
1.9958	3	27	−0.94527	52.2736	−0.3919
2.9996	3	135	−0.33758	78.5645	5.9456
3.1866	3	357	−0.21431	83.4621	8.4741
3.1065	3	1020	0.00349	81.3643	6.7849
3.1420	3	2223	0.00897	82.2945	6.8064
2.0460	5	27	−0.89918	53.5884	−0.2368
2.9380	5	135	−0.32535	76.9521	5.4640
3.3338	5	357	0.19256	87.3178	8.6907
3.1857	5	1020	0.04200	83.4379	7.3824
3.1838	5	2223	0.02963	83.3886	7.2828
3.1420	3	2223	0.00897	82.2945	6.8064
3.1618	4	2223	0.01634	82.8116	7.0626
3.1712	4.5	2223	0.02297	83.0601	7.1948
3.1838	5	2223	0.02963	83.3886	7.2828
3.1930	5.5	2223	0.03401	83.6296	7.3242
(B) Double precision					
3.1069	3	1010	0.00345	81.3739	6.7861
3.3345	5	350	0.19247	87.3362	8.6998
3.1861	5	1010	0.04191	83.4491	7.3856

convergence is the result of an interference of the trigonometric part of the Fourier transform, similar to the process in certain optical problems. The question is, is k large or small compared to what? The sample size and the range of the lattice sum (the range is the radius at which the distribution of points becomes virtually continuous and the angular summation starts to average out) are the only two lengths available.

The point we are interested in, the maximum of $\mathbf{P}(\mathbf{k})$, is probably the point where our type of convergence goes over into the other type. The difficulties are aggravated by the fact that the summation is done on a finite sample rather than on an infinite sample and consequently the maximum of $\mathbf{P}(\mathbf{k})$ may be influenced by the size of the sample. This will influence primarily the position of the maximum, rather than the height.

C. Discussion of Results and Conclusions

1. Entropy

C_2, the second-order correction in the entropy, was found from the direct lattice summation. It is the coefficient of T^{-2} in the entropy series, and is presented in Table IV. We concluded that our best value for C_2 is

$$C_2 = 3.17 \text{ mK}^2,$$

where we made use of the following parameters:

$$a = 11.004 \text{ Å}, \quad g = 1.8286, \quad c/a = 1.572.$$

Hudson, Kaeser, and Radford[20] determined that

$$C_2 = 3.15 \text{ mK}^2.$$

Using values of $a = 10.92$ Å; $g = 1.84$; $c/a = 1.577$, Daniels[6] calculated that

$$C_2 = 3.30 \text{ mK}^2.$$

The small differences in the ratio c/a are of no consequence, but changes in the values of g and a do turn out to be important.

We also utilized the Fourier transform technique to calculate C_2 and arrived at a value of 3.19 mK² for it. This was done to test the accuracy of the Fourier transform method, and the agreement was quite satisfactory, as the two values of C_2 differed by less than 1%.

[20] R. P. Hudson, R. S. Kaeser, and H. E. Radford, in *Proceedings of the Seventh International Conference on Low Temperature Physics, Toronto, 1960* (University of Toronto Press, Toronto, 1961), p. 100.

TABLE IX. Contributions to the entropy from the ring diagrams.

n	I_1	I_2	I_1+I_2	Same by direct Σ	$\dfrac{(I_1+I_2)(-1)^{n+1}}{}\times\dbinom{n-1}{2n}\left(\dfrac{g^2\mu_B{}^2 10^3}{4Ka^3}\right)^n$
1	5.1789	-5.1449	0.03401	0.00	$\cdots$
2	5.2212×10^1	3.1411×10^1	8.3630×10^1	82.96	-3.193
3	5.8122×10^2	-2.1306×10^2	3.6816×10^2	348.68	$+7.324$
4	7.3909×10^3	1.5460×10^3	8.9369×10^3	$\cdots$	-7.824×10^1
5	1.0060×10^5	-1.1737×10^4	8.8864×10^4	$\cdots$	$+3.240\times10^2$
6	1.4566×10^6	9.204×10^4	1.5487×10^6	$\cdots$	-2.298×10^3
7	2.2061×10^7	-7.396×10^5	2.1321×10^7	$\cdots$	$+1.272\times10^4$
8	3.4680×10^8	6.058×10^6	3.5286×10^8	$\cdots$	-8.398×10^4
9	5.6147×10^9	-7.037×10^7	5.5643×10^9	$\cdots$	$+5.273\times10^5$
10	9.3111×10^{10}	4.240×10^8	9.3535×10^{10}	$\cdots$	-3.497×10^6

C_3, the third-order coefficient, was also determined by the two methods, and the result of the direct lattice summation was

$$C_3 = -6.94 \text{ mK}^3.$$

Using the Fourier transform, the third-order correction turned out to be equal to -7.32 mK^3, so these two values of C_3 differed by about 5%.

It is not practical to attempt higher-order corrections by means of the direct lattice summation in view of the computer time required. As a consequence, only the Fourier transform approach was utilized for the fourth- and higher-order corrections. We found that

$$C_4 = 78.2 \text{ mK}^4.$$

The value of this coefficient is somewhat uncertain for we estimated diagrams (4-2) and (4-3)b were of no importance and determined (4-3)a to yield a 10% correction.

As far as higher-order corrections are concerned, we consider them as too unreliable to quote at present.

2. Susceptibility

$P^{\alpha\beta}(\mathbf{k})$ attains its minimum value in a "staggered field" at $k_x = 1.225$, $k_y = 0$, $k_z = 0$ (a point which is degenerate with two other points in the XOZ plane). This minimum, $P^{yy}(\mathbf{k}) = -8.888$ in units of $a = 1$ with $c/a = 1.5718$, and it results in a Curie-Weiss Δ such that

$$\Delta = 3.474 \text{ mK}.$$

ACKNOWLEDGMENT

APPENDIX A: CONTRIBUTIONS TO SUSCEPTIBILITY

The explicit contributions for the fourth and fifth-order diagrams in the susceptibility are

(4.2)a: $\quad 3\sum'_{i,j} P_{ij}{}^{\alpha\beta}P_{ij}{}^{\alpha\beta}(\mu_i{}^\alpha\mu_i{}^\alpha + \mu_j{}^\alpha\mu_j{}^\alpha)$

$$+\sum_{i,j\,\alpha\neq\gamma} P_{ij}{}^{\alpha\beta}P_{ij}{}^{\alpha\beta}(\mu_i{}^\gamma\mu_i{}^\gamma + \mu_j{}^\gamma\mu_j{}^\gamma)$$

$$+2\sum_{i,j\,\alpha\neq\gamma} P_{ij}{}^{\alpha\beta}P_{ij}{}^{\alpha\beta}(\mu_i{}^\alpha\mu_i{}^\gamma + \mu_j{}^\alpha\mu_j{}^\gamma),$$

(4.2)b: $\quad \sum P_{ij}{}^{\delta\gamma}P_{ij}{}^{\delta\gamma}\mu_i{}^\rho\mu_j{}^\tau\epsilon_{\alpha\delta\rho}\epsilon_{\beta\gamma\tau},$

(5.2): $\quad \sum [P_{ij}{}^{\alpha\beta}P_{ij}{}^{\alpha\beta}P_{ij}{}^{\alpha\beta}(\mu_i{}^\delta\mu_j{}^\gamma + \mu_i{}^\gamma\mu_j{}^\delta)],$

(5.3)a: $\quad \sum [P_{ij}{}^{\alpha\beta}P_{jk}{}^{\beta\delta}P_{ki}{}^{\delta\gamma}\mu_i{}^\alpha\mu_i{}^\gamma$

$$+P_{ij}{}^{\alpha\beta}P_{jk}{}^{\delta\gamma}P_{ki}{}^{\gamma\alpha}\mu_j{}^\beta\mu_j{}^\delta$$

$$+P_{ij}{}^{\alpha\beta}P_{jk}{}^{\beta\gamma}P_{ki}{}^{\delta\alpha}\mu_k{}^\alpha\mu_k{}^\gamma]$$

$$+\sum [P_{ij}{}^{\alpha\beta}P_{jk}{}^{\beta\gamma}P_{ki}{}^{\gamma\alpha}(\mu_i{}^\rho\mu_i{}^\rho + \mu_j{}^\rho\mu_j{}^\rho + \mu_k{}^\rho\mu_k{}^\rho)],$$

(5.3)b: $\quad \sum (2P_{ij}{}^{\alpha\beta}P_{jk}{}^{\delta\gamma}P_{jk}{}^{\beta\gamma}\mu_i{}^\alpha\mu_j{}^\delta$

$$+P_{ij}{}^{\alpha\beta}P_{jk}{}^{\delta\gamma}P_{jk}{}^{\delta\gamma}\mu_i{}^\alpha\mu_j{}^\beta),$$

(5.3)c: $\quad -\sum P_{ij}{}^{\alpha\beta}P_{jk}{}^{\delta\gamma}P_{jk}{}^{\nu\eta}\mu_i{}^\alpha\mu_k{}^\rho\epsilon_{\rho\gamma\eta}\epsilon_{\beta\delta\nu},$

(5.3)d: $\quad\quad$ zero,

(5.3)e: $\quad\quad$ zero,

(5.3)f: $\quad \sum \epsilon_{\alpha\delta\eta}P_{ij}{}^{\alpha\beta}P_{ij}{}^{\delta\beta}P_{ij}{}^{\eta\gamma}(\mu_i{}^\beta\mu_i{}^\rho + \mu_j{}^\beta\mu_j{}^\rho)$

$$+P_{ij}{}^{\alpha\beta}P_{ij}{}^{\delta\rho}P_{ij}{}^{\eta\gamma}(\mu_i{}^\beta\mu_i{}^\beta + \mu_j{}^\beta\mu_j{}^\beta).$$

The symbol ϵ is the Levi-Civita symbol.

APPENDIX B: INTEGRAL APPROXIMATION

We would like to examine the following integral approximation:

$$\lim_{n\to\infty} \sum_i^n P^{xx}(r_{ij})\cos(\mathbf{k}\cdot\mathbf{r}) = \sum_i^{n(R)} P^{xx}(r_{ij})\cos(\mathbf{k}\cdot\mathbf{r}_{ij})$$

$$+\frac{1}{V}\int_R^\infty P^{xx}(r)\cos(\mathbf{k}\cdot\mathbf{r})d\mathbf{r}, \quad \text{(B1)}$$

where V is the volume occupied by one ion on the average. The left hand side of the above equation is equal to $P^{xx}(\mathbf{k})$, which explains the motivation for this Appendix.

To begin with, $P^{xx}(r)$ is given by

$$P^{xx}(r) = (3 \sin^2\theta \cos^2\varphi - 1)/r^3. \qquad (B2)$$

Equation (B2) can be rewritten in terms of spherical harmonics as

$$P^{xx}(r) = \frac{3(2\pi/15)^{1/2}(y_2{}^2 + y_2{}^{2*}) - (4\pi/5)^{1/2}y_2{}^0}{r^3} \qquad (B3)$$

The following three well-known relations will be utilized in this development:

$$e^{i\mathbf{k}\cdot\mathbf{r}} = 4\pi \sum_{l=0}^{\infty} \sum_{m=-l}^{l} i^l j_l(kr)$$

$$\times y_l{}^{m*}(\theta_k, \varphi_k) y_l{}^m(\theta_r, \varphi_r), \qquad (B4)$$

$$\int y_l{}^{m*} y_{l'}{}^{m'} d\Omega = \delta_{mm'}\delta_{ll'}, \qquad (B5)$$

$$\cos(\mathbf{k}\cdot\mathbf{r}) = \tfrac{1}{2}(e^{i\mathbf{k}\cdot\mathbf{r}} + e^{-i\mathbf{k}\cdot\mathbf{r}}), \qquad (B6)$$

where $j_l(kr)$ is the spherical Bessel function; θ_k and φ_k are the polar angles specifying the orientation of the vector $\mathbf{k}$; θ_r and φ_r perform a similar service for $\mathbf{r}$.

The first step in the evaluation of the integral in Eq. (B1) is to substitute Eq. (B3) for $P^{xx}(r)$; then Eqs. (B4) and (B6) are invoked to replace $\cos(\mathbf{k}\cdot\mathbf{r})$ the orthonormality relation for the spherical harmonics, Eq. (B5), enables us to write that

$$\frac{1}{V} \int_R^\infty \int_0^{2\pi} \int_0^\pi P^{xx}(r) \cos(\mathbf{k}\cdot\mathbf{r}) \, d\mathbf{r}$$

$$= 4\pi\{(4\pi/5)^{1/2}y_2{}^0(\theta_k,\varphi_k) - 3(2\pi/15)^{1/2}$$

$$\times [y_2{}^2(\theta_k,\varphi_k) + y_2{}^{2*}(\theta_k,\varphi_k)]\}$$

$$\times \frac{1}{V} \int_R^\infty \frac{j_2(kr)dr}{r}$$

$$= \frac{2\pi}{V}[3 \cos^2\theta_k - 1 + 3 \sin^2\theta_k(2 \sin^2\varphi_k - 1)]$$

$$\times \int_R^\infty \frac{j_2(kr)dr}{r}. \qquad (B7)$$

The integral in Eq. (B7) is given by

$$\int_R^\infty \frac{j_2(kr)dr}{r} = \frac{3}{k^3} \int_R^\infty \frac{\sin kr \, dr}{r^4} - \frac{1}{k} \int_R^\infty \frac{\sin kr \, dr}{r^2}$$

$$- \frac{3}{k^2} \int_R^\infty \frac{\cos kr \, dr}{r^3}. \qquad (B8)$$

After performing three successive integrations by parts on the first term on the right-hand side of Eq. (B8), we can express the integral as follows:

$$\frac{3}{k^3} \int_R^\infty \frac{\sin kr \, dr}{r^4} = -\frac{\sin kr}{(kr)^3}\Big|_R^\infty - \frac{\cos kr}{2(kr)^2}\Big|_R^\infty$$

$$+ \frac{\sin kr}{2kr}\Big|_R^\infty - \frac{1}{2} \int_R^\infty \frac{\cos kr \, dr}{r}.$$

Therefore,

$$\frac{3}{k^3} \int_R^\infty \frac{\sin kr \, dr}{r^4} = \frac{\sin kR}{(kR)^3} + \frac{\cos kR}{2(kR)^2}$$

$$- \frac{\sin kR}{2kR} - \frac{1}{2} \int_R^\infty \frac{\cos kr \, dr}{r}. \qquad (B9)$$

Only one integration by parts on the second term on the right-hand side of Eq. (B7) is needed to show that

$$-\frac{1}{k} \int_R^\infty \frac{\sin kr \, dr}{r^2} = -\frac{\sin kR}{kR} - \int_R^\infty \frac{\cos kr \, dr}{r}. \qquad (B10)$$

Two integrations by parts enable us to write the last term in Eq. (B8) as

$$\frac{-3}{k^2} \int_R^\infty \frac{\cos kr \, dr}{r^3} = -\frac{3 \cos kR}{2(kR)^2} + \frac{3 \sin kR}{2kR}$$

$$+ \frac{3}{2} \int_R^\infty \frac{\cos kr \, dr}{r}. \qquad (B11)$$

If we add Eqs. (B9)–(B11), and then substitute the result into Eq. (B8), we discover that the integrals cancel, and therefore,

$$\int_R^\infty \frac{j_2(kr)dr}{r} = \frac{\sin kR}{(kR)^3} - \frac{\cos kR}{(kR)^2}. \qquad (B12)$$

Finally, utilizing Eqs. (B12) and (B7) in Eq. (B1), we have

$$\lim_{n\to\infty} \sum_i^n P^{xx}(r_{ij}) \cos(\mathbf{k}\cdot\mathbf{r}_{ij}) = \sum_i^{n(R)} P^{xx}(r_{ij}) \cos(\mathbf{k}\cdot\mathbf{r}_{ij})$$

$$+ \frac{2\pi}{V}[3 \cos^2\theta_k - 1 + 3 \sin^2\theta_k(2 \sin^2\varphi_k - 1)]$$

$$\times \left[\frac{\sin kR}{(kR)^3} - \frac{\cos kR}{(kR)^2}\right]. \qquad (B13)$$